energies

MDPI

Article

Analysis and Verification of Equivalent Circuit Model of Soft-Pack Lithium Batteries

Fei Li [1,2], Zhaojie Li [1,2], Yanlei Zhang [1,*], Guoning Xu [1], Xuwei Wang [1] and Haoyi Zhang [3]

[1] Aerospace Information Research Institute, Chinese Academy of Sciences, Beijing 100094, China
[2] University of Chinese Academy of Sciences, Beijing 100049, China
[3] Leicester International Institute, Dalian University of Technology, Panjin 124221, China
* Correspondence: zhangyanlei@aoe.ac.cn

Abstract: High-energy-density lithium batteries play a crucial role in the lightweight design of stratospheric airship systems. This paper conducts an in-depth experimental study of the equivalent circuit model of soft-pack batteries, with a focus on how parameter identification methods affect model accuracy. To this end, first-order RC, second-order RC, and third-order RC equivalent circuit models were constructed, and model parameters under different temperature and current conditions were obtained through constant-current intermittent discharge experiments. During the parameter identification process, special consideration was given to the impact of sampling time on voltage measurements and the interdependent constraints among models. Additionally, the effects of current, temperature, and SOC (state of charge) variations on ohmic resistance and polarization resistance–capacitor parameters were analyzed. The experimental results show that the root mean square error (RMSE) of battery terminal voltage calculated using parameter identification methods that account for these factors is significantly lower than when these factors are not considered. By comparing the voltage calculation accuracy and operational efficiency of the three models, the second-order RC model was determined to be the preferred choice due to its simple structure, high computational efficiency, and superior accuracy.

Keywords: soft-pack lithium battery; n-RC equivalent circuit model; parameter identification

check for updates

Academic Editor: Carlos Miguel Costa

Received: 13 December 2024
Revised: 16 January 2025
Accepted: 21 January 2025
Published: 23 January 2025

Citation: Li, F.; Li, Z.; Zhang, Y.; Xu, G.; Wang, X.; Zhang, H. Analysis and Verification of Equivalent Circuit Model of Soft-Pack Lithium Batteries. *Energies* **2025**, *18*, 510. https://doi.org/10.3390/en18030510

Copyright: © 2025 by the authors. Licensee MDPI, Basel, Switzerland. This article is an open access article distributed under the terms and conditions of the Creative Commons Attribution (CC BY) license (https://creativecommons.org/licenses/by/4.0/).

1. Introduction

Compared to traditional hard-shell batteries, soft-pack batteries (typically encapsulated in aluminum–plastic film) have drawn significant attention from researchers in the field of stratospheric airships due to their advantages such as high energy density, excellent stability, long cycle life, and superior safety performance [1,2]. Stratospheric airships are a new type of near-space solar-powered aircraft that store excess energy in energy storage batteries during the day and utilize this stored energy at night to maintain propulsion and the operation of onboard equipment [3–5]. High-performance batteries play a crucial role in improving the wind resistance, flight endurance, and energy efficiency of stratospheric airships [6–8].

Generally, the greater the energy storage capacity of the batteries, the stronger the airship's wind resistibility and maneuverability. Although the energy system is one of the most crucial subsystems of a stratospheric airship, the allowed weight and volume remain highly constrained. As a result, developers are seeking to adopt advanced battery technologies with higher energy density to enhance energy supply ability. In the foreseeable future, soft-pack batteries will be regarded as the most promising solution [9].

Before applying a new piece of technology, it is essential to understand its characteristics. Equivalent circuit modeling [10] is often used to depict the dynamic characteristics of a battery. It simulates the actual response of a battery using basic electronic components such as resistors and capacitors. The limited number of and easily identifiable parameters make it easy to implement in engineering practice [11]. A basic and well-known equivalent circuit for battery is the Rint model, which connects the battery with an ideal voltage source and an internal resistor in the series. The structure of the Rint model is too simple, not considering polarization and diffusion phenomena, and thus, it can only reflect a part of the operating characteristics of a battery [12]. To improve the accuracy of the model, researchers have extended the basic Rint model by adding varying numbers of resistor–capacitor (RC) series–parallel networks, leading to the development from first-order RC equivalent circuit models to more precise multi-order RC equivalent circuit models, collectively referred to as n-RC equivalent circuit models [13–15].

Most of the previous literature on battery modeling has been on hard-shell batteries. The first-order RC model proposed by Liaw et al. [16] is widely used in battery modeling, which is accurate in describing the external characteristics and can accurately simulate battery behaviors. Xia et al. [17] used a second-order RC equivalent circuit to approximate the battery's dynamic performance. Wang et al. [18] found that a second-order RC equivalent circuit shows better prediction performance than that of a first-order RC equivalent circuit for a LiNCM cell. Hu et al. [19] provided a comprehensive comparison of twelve equivalent circuits. Wang et al. [20–22] noted that the model accuracy of the third-order to the fifth-order RC networks did not greatly change. They studied the characteristics of lithium batteries based on the third-order RC equivalent circuit model. Xia et al. [23] proposed a variable-order RC equivalent circuit model that varied in the first, second, and third orders. Lin et al. [24] argued that the second-order RC equivalent circuit model had higher accuracy and was not much more complicated than Thevenin's model (the first-order RC equivalent circuit model), although it has one more RC link. Amir et al. [25] found that the second-order RC equivalent circuit model was more accurate than the first-order and nth-order RC equivalent circuit models in their study of the battery capacity (SOH). Pande et al. [26] concluded that among the RC equivalent models with different orders, the third-order RC equivalent model had better dynamic results for the estimation of the internal parameters of a battery.

In addition to studies of the structure of the model itself, some have investigated the effect of the internal states or external environment on the model parameters. Various factors, such as the operating current, temperature, and state of charge (SOC), can significantly influence model parameters [27,28]. Damodaran et al. proposed that resistance–capacitance (RC) parameters are dependent on SOC and ambient temperature. Accurately estimating these parameters is essential for developing a robust equivalent circuit model [29]. Guo et al. performed pulse discharge tests under different ambient temperatures to obtain data that were used to fit the resistance and capacitance parameters of a 2-RC equivalent circuit model [30]. Meanwhile, Yoganandan et al. developed electro-thermal models for lithium-ion batteries using both 1-RC and 2-RC configurations. They conducted performance comparisons to assess the voltage accuracy of these models, highlighting the advantages and limitations of each approach [31]. Furthermore, Surya et al. utilized first-order and second-order thermal models based on thermal resistance–capacitance networks to estimate core and surface temperatures in lithium-ion battery stacks, thereby providing insights into thermal management strategies [32]. Wang and Bairwa analyzed the effects of temperature and the SOC [33,34], whereas Barletta and Duru focused on the impacts of the discharge rate and SOC [35,36].

However, the applicability of existing equivalent circuit models must be experimentally studied and verified before actual application. Existing studies have tended to ignore the effect of the packaging method on battery performance. Prior research has been centered on hard-shell batteries, with less attention paid to soft-pack batteries. The structure and material properties impact the model parameters, mainly the internal resistance, including the ohmic resistance and polarization resistance. Soft-pack batteries typically have lower internal resistance than hard-shell ones because soft-pack batteries have flexible packaging and less internal support structure. Additionally, few studies have paid attention to the interdependent constraints between RC circuit models of different orders.

Aiming to support the engineering application performance advancement of stratospheric airships, we comparatively investigated the applicability of RC equivalent circuit models of various orders for aluminum–plastic film-encapsulated soft-pack lithium battery. The effects of various temperatures and discharge rates on battery performance were considered, with reliable data obtained through a designed constant-current intermittent discharge experiment. On this basis, the first-, second-, and third-order RC equivalent circuit models were systematically analyzed, and the relationships among the model parameters were discussed. Accurate parameter identification was also performed. By comparing the performances of the models, the most suitable battery model for engineering applications was determined. This study provided solid theoretical support and valuable guidance for the development and practical application of high-energy-density soft-pack lithium batteries on stratospheric airships.

2. n-RC Equivalent Circuit Model

In the field of modeling electrochemical energy systems, RC circuits are widely used to construct equivalent circuit models to characterize the polarization properties of batteries. Based on the Rint equivalent circuit model, which consists of only a resistor and a voltage source, an n-RC equivalent circuit model that accurately reflects the characteristics of lithium batteries can be formed by adding the series–parallel RC circuits of different orders.

Figure 1 shows the n-RC equivalent circuit model. It consists of three parts: the equivalent voltage source, i.e., the open-circuit voltage UOCV of the battery; ohmic resistor R0; and RC circuits, i.e., the polarization resistors and capacitors R_1, C_1, . . ., R_n, C_n.

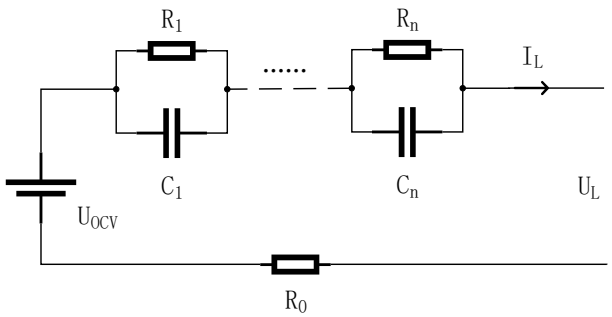


Figure 1. Model diagram of the n-RC equivalent circuit.

The terminal voltage of the polarization RC is U_1 (corresponding to R_1, C_1) . . . U_n (corresponding to R_n and C_n), the load terminal voltage is U_L, and the terminal current is I_L.

We considered moments t and t−1 with time interval tc. Based on Kirchhoff's law and the battery model, we derived the equation for the terminal voltages as follows:

$$\begin{cases} U_{1,t} = e^{\frac{-t_c}{R_1 C_1}} \times U_{1,t-1} + R_1\left(1 - e^{\frac{-t_c}{R_1 C_1}}\right) \times I_{L,t-1} \\ \vdots \\ U_{n,t} = e^{\frac{-t_c}{R_n C_n}} \times U_{n,t-1} + R_n\left(1 - e^{\frac{-t_c}{R_n C_n}}\right) \times I_{L,t-1} \end{cases} \quad (1)$$

$$U_{L,t} = U_{OCV,t} - U_{1,t} \cdots - U_{n,t} - R_0 I_{L,t} \quad (2)$$

3. Parameter Identification Experiment

For the commonly used n-RC equivalent circuit models, i.e., first-, second-, and third-order RC equivalent circuit models [37,38], we performed parameter identification to verify the accuracy of the open-circuit voltage algorithm. The models are shown in Figure 2 as ①, ②, and ③.

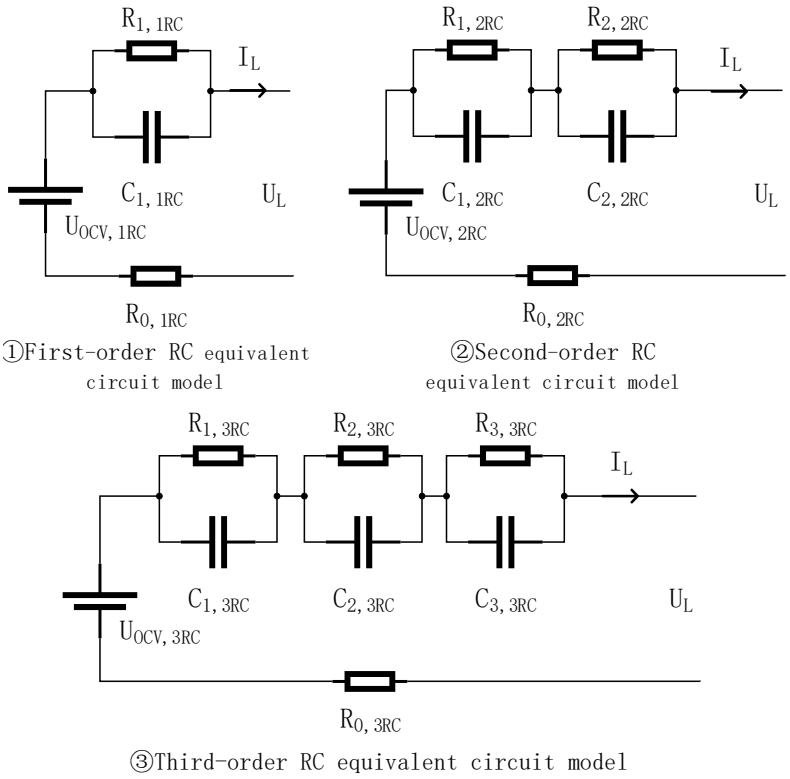


Figure 2. Common n-RC equivalent circuit model.

The parameters of these three models consist of three parts: open-circuit voltage, ohmic resistance, polarization resistance and polarization capacitance. Considering the typical flight condition of stratospheric airships, we designed the parameter identification experiments under different temperatures and discharge C rates.

3.1. Constant-Current Intermittent Discharge Experiment

We used the constant-current intermittent discharge (CCID) [39] method to perform a series of discharge experiments on the battery under different temperatures and discharge C rates. Figure 3 shows the specific experimental steps.

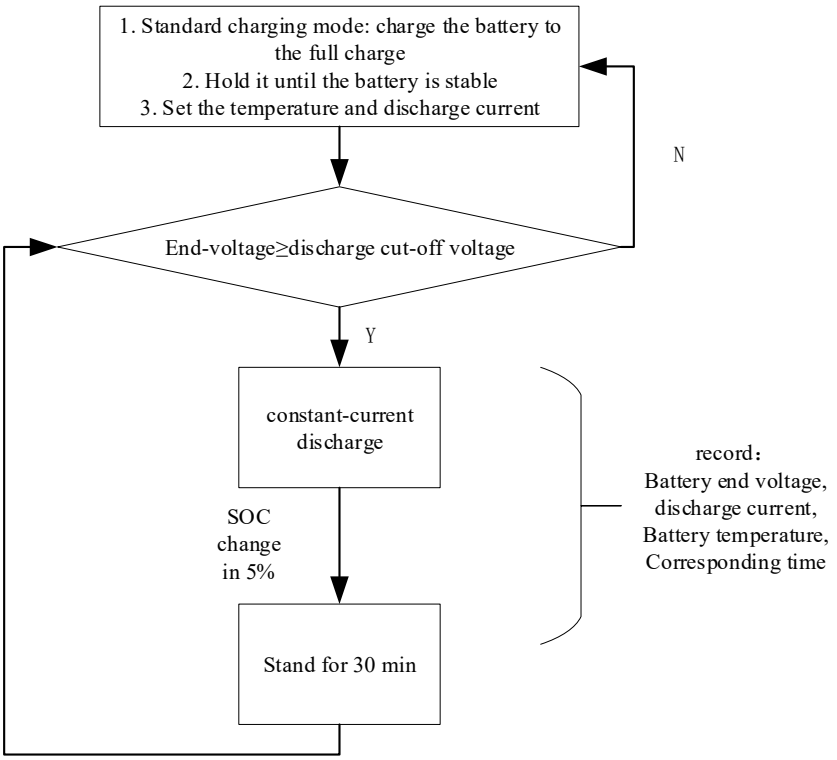


Figure 3. Flowchart of the constant-current intermittent discharge experiment.

The selected temperature range was 0–30 °C, and there was one measurement every 5 °C, so there were seven different temperature measurement conditions in total. The average discharge rate in a real flight mission is typically below 0.1 C. Taking into account the effects of load dynamics, the short-term maximum discharge rate does not exceed 0.5 C, so the range of the discharge rate was set to 0.05–0.5 C with a step of 0.05 C. Considering the temperature and discharge C rate together, 70 groups of measurement conditions were set. Table 1 shows the settings of the operating temperature, battery discharge C rate and rest time of the battery pack in the experiment.

Table 1. Constant-current intermittent discharge parameters.

Parameters	Numerical Value
Temperature	0–30 °C with 5 °C interval step
Discharge C rate	0.05–0.5 C in 0.05 C interval steps
Discharge time	3 min/discharge rate (time required for 5% change in SOC)
Rest time	30 min

To ensure the data accuracy, each measurement condition had two batteries for the constant-current intermittent discharge experiment. The data accuracy was verified by comparing the changes in terminal voltages. Since there were 70 groups of measurement conditions, 140 groups of constant-current intermittent discharge tests were conducted, and 140 groups of constant-current intermittent discharge data were obtained.

3.2. Experiment Platform

In this work, we used a 30 Ah, 320 Wh/kg high-energy-density soft-pack lithium battery as the test object. The experiment platform consists of a host computer, acquisition equipment (a temperature acquisition card and voltage acquisition card), charging and

discharging equipment (DC power supply and DC electronic load), an ordinal temperature (0–60) box, and a host computer. Table 2 shows the relevant parameters of the battery.

Table 2. Soft-pack lithium battery cell parameters.

Items	Value
Nominal capacity	30 Ah
Nominal voltage	3.65 V
Anode material	NCM811
Cathode material	Silicon Carbon (15% silicon)
Electrolyte	LiPF6,LiFSI
Charge cutoff voltage	4.3 V
Discharge cutoff voltage	2.7 V

Figure 4 shows the circuit connection diagram. We placed the battery in the temperature control box, passed the lead through the test holes, and connected the battery under testing to the data acquisition equipment and charging/discharging equipment. The acquired data were transmitted to the host computer.

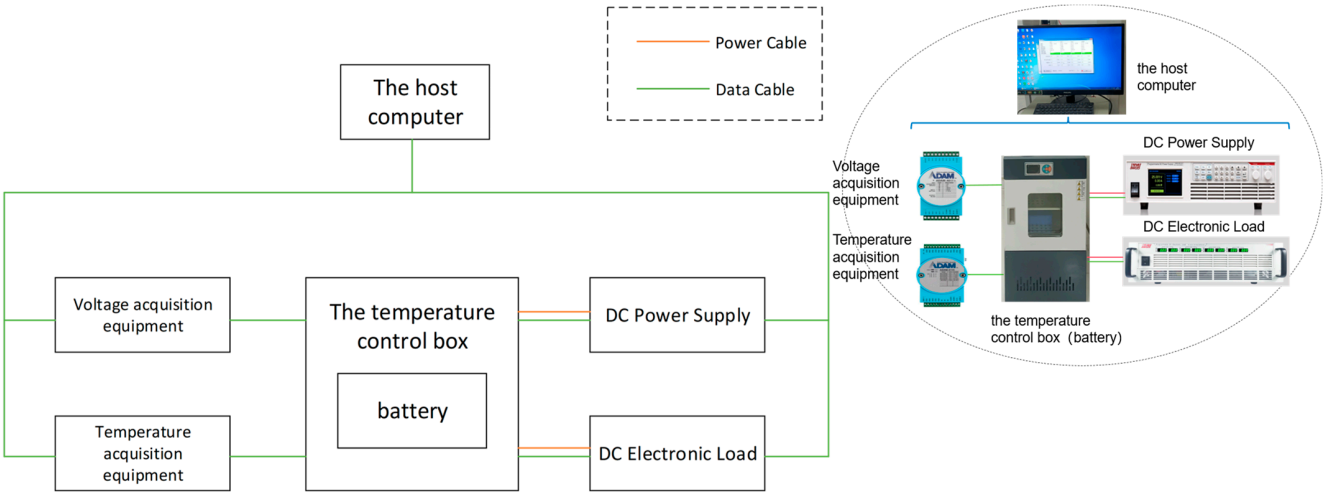
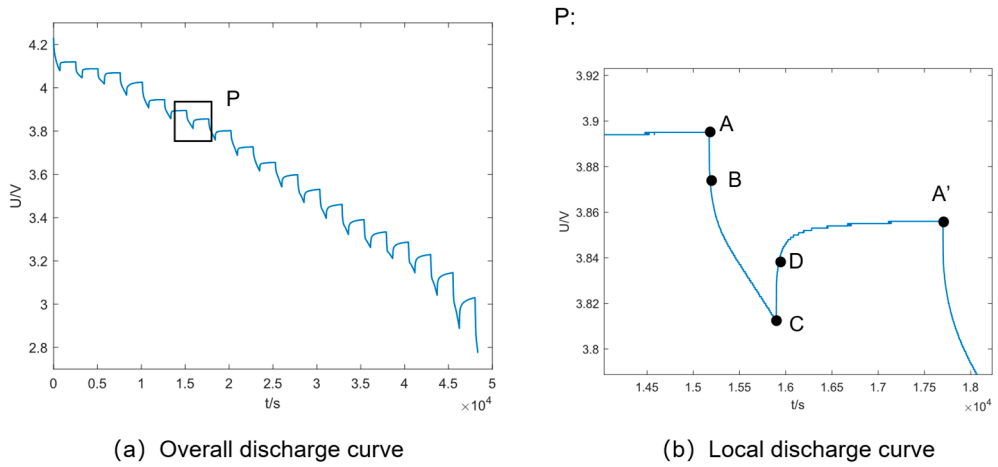


Figure 4. Circuit connection diagram of the constant-current intermittent discharge experiment.

4. Model Parameter Identification

Parameter identification is closely related to the constant-current intermittent discharge terminal voltage curve. By analyzing the constant-current intermittent discharge terminal voltage curve, the electrochemical property of lithium batteries can be understood, and information about the electrochemical behavior of lithium batteries can be provided. Parameter identification can convert the information provided by the intermittent discharge terminal voltage curve into the parameters of the equivalent circuit model to simulate, predict and evaluate lithium batteries.

Due to the large number of data groups, we randomly selected one of the 140 data groups to plot the battery terminal voltage curve and took one of the discharge–rest process curves as an example for the analysis. Figure 5 shows the terminal voltage curve at 25 °C and 6 A (0.2 C), where A→C is the battery discharge process, and C→A′ is the rest process. When the battery began to discharge, there was a sudden decrease in voltage, i.e., A→B. When the battery stopped discharging, there was a sudden increase in voltage, i.e., C→D.



(a) Overall discharge curve (b) Local discharge curve

Figure 5. Variation in terminal voltage with time obtained from the intermittent discharge experiment.

During the discharge process, when the discharge begins, the battery voltage drops sharply, rapidly decreasing from point A to point B. After this initial decline, the voltage change becomes more gradual and begins to stabilize, resulting in a slower rate of voltage decrease. As the discharge approaches completion, the battery voltage reaches point C, marking the transition to the resting stage.

Toward the end of the discharge, the battery voltage shows a significant surge, quickly returning to point D. As the resting period continues, the voltage rises slightly and eventually stabilizes at a new level, referred to as point A′.

An analysis of the discharge curves enables one to derive three types of model parameters: open-circuit voltage, ohmic resistance, and polarization resistance and polarization capacitance. The method is as follows:

(1) Open-circuit voltage UOCV

After a period of rest, the internal electrochemical properties of the battery gradually stabilized. At this time, the internal polarization basically had no effect on the battery. The identified battery terminal voltage (the voltage at point A) was the open-circuit voltage.

(2) Ohmic resistance R0

Batteries have sudden voltage changes at the beginning of discharge (AB section) and end of discharge (CD section). At the instant when the discharge/charge begins, the RC circuit does not produce a large voltage change due to the capacitance, whereas the voltage of the ohmic resistor will abruptly change due to the change in current. Combined with Equation (2), according to Ohm's law, the ohmic resistance can be derived as shown in Equation (3), i.e., ohmic resistance R_0 can be calculated from the voltage difference between points A and B or between points D and C and the corresponding current.

$$R_0 = \frac{U_{L,A} - U_{L,B}}{I_L} = \frac{U_{L,D} - U_{L,C}}{I_L} \tag{3}$$

(3) Polarization resistance and polarization capacitance

In the process of D→A′, the battery is in a static state. Since the current is 0, the corresponding voltage of the ohmic resistor is also 0. At this time, the change in terminal voltage is mainly generated by the capacitor discharge, and the terminal voltage is shown in Equation (4).

$$U_{L,t} = U_{OCV} - I_L R_1 e^{\frac{-t_c}{R_1 C_1}} - \cdots - I_L R_n e^{\frac{-t_c}{R_n C_n}} \tag{4}$$

From Equation (4), at point D, since tc is 0, the terminal voltage at this point is shown in Equation (5).

$$U_{L,D} = U_{OCV} - I_L R_1 - \cdots - I_L R_n \quad (5)$$

Since point A′ is an open-circuit voltage, combined with Equation (5), Equation (6) can be obtained.

$$U_{L,A'} - U_{L,D} = I_L R_1 + \cdots + I_L R_n \quad (6)$$

Due to the sampling interval in the experiment, there was a time difference of at least 1 s between two sampling points. Because the corresponding voltage of the ohmic resistor changes when the current changes, the actual D point should be between points C and D′ (the voltage corresponding to its next instant), as shown in Figure 6.

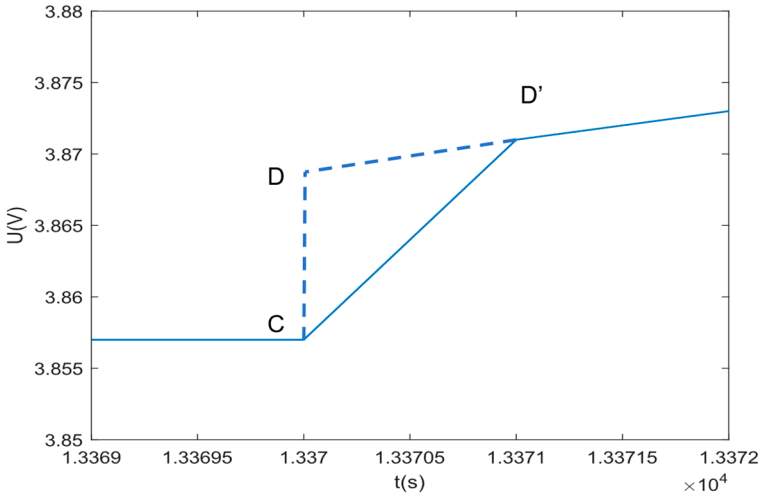


Figure 6. Illustration of the position of points C, D and D′.

t_D is the time difference between point C and its next instant. The voltage difference between point C and point D′ is caused by two main factors. First, the voltage drop from point C to point D is due to the internal ohmic resistance of the battery, reflecting its instantaneous response when the discharge current is applied. Second, the voltage change from point D to point D′ results from the discharge behavior of the internal polarized capacitor during the t_D period. Together, these two voltage changes account for the overall voltage difference between point C and point D′.

$$U_{L,D'} - U_{L,C} = I_L R_0 + I_L R_1 e^{\frac{-t_D}{R_1 C_1}} + \cdots + I_L R_n e^{\frac{-t_D}{R_n C_n}} \quad (7)$$

By combining Equations (3) and (6), the voltage difference between point A′ and point C can be derived, as shown in Equation (8).

$$U_{L,A'} - U_{L,C} = I_L R_0 + I_L R_1 + \cdots + I_L R_n \quad (8)$$

During the transition from point D′ to A′, the time constant t_C is set to zero at point D′. Since the voltage change from point D to point D′ is accounted for between points C and D′, the actual starting point of the influence caused by the discharge of the polarizing capacitor should be point D. Consequently, by the time the system reaches point D′, the polarizing capacitor has already undergone a discharge process lasting t_D. Therefore, the terminal voltage formula for this stage can be adjusted as per Equation (9).

$$U_{L,t} = U_{OCV} - I_L R_1 e^{\frac{-t_D - t_C}{R_1 C_1}} - \cdots - I_L R_n e^{\frac{-t_D - t_C}{R_n C_n}} \quad (9)$$

On the other hand, different models should exhibit similar external characteristics. Therefore, the ohmic resistance values of models with different orders should remain consistent, and their terminal voltage expressions should also constrain each other. The following constraints were set to accurately obtain the resistance and capacitance parameters of the first-, second-, and third-order RC equivalent circuit models, as shown in Equations (10) and (11):

$$U_{L,A'} - U_{L,C} = \begin{cases} I_L R_0 + I_L R_{1,1RC} \\ I_L R_0 + I_L R_{1,2RC} + I_L R_{2,2RC} \\ I_L R_0 + I_L R_{1,3RC} + I_L R_{2,3RC} + I_L R_{3,3RC} \end{cases} \quad (10)$$

$$U_{L,D'} - U_{L,C} = \begin{cases} I_L R_0 + I_L R_{1,1RC} e^{\frac{-t_D}{R_{1,1RC} C_{1,1RC}}} \\ I_L R_0 + I_L R_{1,2RC} e^{\frac{-t_D}{R_{1,2RC} C_{1,2RC}}} + I_L R_{2,2RC} e^{\frac{-t_D}{R_{2,2RC} C_{2,2RC}}} \\ I_L R_0 + I_L R_{1,3RC} e^{\frac{-t_D}{R_{1,3RC} C_{1,3RC}}} + I_L R_{2,3RC} e^{\frac{-t_D}{R_{2,3RC} C_{2,3RC}}} + I_L R_{3,3RC} e^{\frac{-t_D}{R_{3,3RC} C_{3,3RC}}} \end{cases} \quad (11)$$

The fitting function of the ohmic and polarization resistances and capacitances is shown in Equation (12); the parameters to be fitted were R_0, $R_{1,1RC}$, $C_{1,1RC}$, $R_{1,2RC}$, $C_{1,2RC}$, $R_{2,2RC}$, $C_{2,2RC}$, $R_{1,3RC}$, $C_{1,3RC}$, $R_{2,3RC}$, $C_{2,3RC}$, $R_{3,3RC}$, and $C_{3,3RC}$.

$$U_{L,t} = \begin{cases} U_{OCV} - I_L R_{1,1RC} e^{\frac{-t_D - t_c}{R_{1,1RC} C_{1,1RC}}} \\ U_{OCV} - I_L R_{1,2RC} e^{\frac{-t_D - t_c}{R_{1,2RC} C_{1,2RC}}} - I_L R_{2,2RC} e^{\frac{-t_D - t_c}{R_{2,2RC} C_{2,2RC}}} \\ U_{OCV} - I_L R_{1,3RC} e^{\frac{-t_D - t_c}{R_{1,3RC} C_{1,3RC}}} - I_L R_{2,3RC} e^{\frac{-t_D - t_c}{R_{2,3RC} C_{2,3RC}}} - I_L R_{3,3RC} e^{\frac{-t_D - t_c}{R_{3,3RC} C_{3,3RC}}} \end{cases} \quad (12)$$

The upper limit of the ohmic resistance was set as $(U_{L,D'} - U_{L,C})/I_L$, and the upper limit of the polarization resistance was set as $(U_{L,A'} - U_{L,C})/IL$. Since the polarization capacitance was generally in the order of kilofarads, the upper limit of the polarization capacitance was set to be 500 kF. Meanwhile, since different initial values greatly impact the fitting results, for the same set of data, by choosing different initial values, we obtained multiple sets of data (100 sets); we compared the results and selected the one with the smallest error as the relatively accurate resistance parameter.

Figure 7 shows the variation in the ohmic resistance (R0). The data indicate that the ohmic resistance of soft-pack lithium batteries remains relatively stable except at low currents. Temperature and the state of charge (SOC) have minimal influence on ohmic resistance. However, changes in current, especially at low currents, can lead to a significant reduction in ohmic resistance.

Figure 8 shows the correlation graphs of the polarization resistances $R_{1,1RC}$, $R_{1,2RC}$, $R_{2,2RC}$, $R_{1,3RC}$, $R_{2,3RC}$, and $R_{3,3RC}$. It is evident from the figure that the polarization resistance exhibits relatively stable characteristics, only increasing to a certain extent under low-current and low-SOC conditions. Additionally, when the temperature is low, the polarization resistance is relatively high, but the difference is not significant.

Figure 9 illustrates the correlation graphs of the polarization capacitances $C_{1,1RC}$, $C_{1,2RC}$, $C_{2,2RC}$, $C_{1,3RC}$, $C_{2,3RC}$, and $C_{3,3RC}$. As shown in the figure, compared to resistance,

the changes in polarization capacitance are more random. However, most of the capacitance values remain relatively stable.

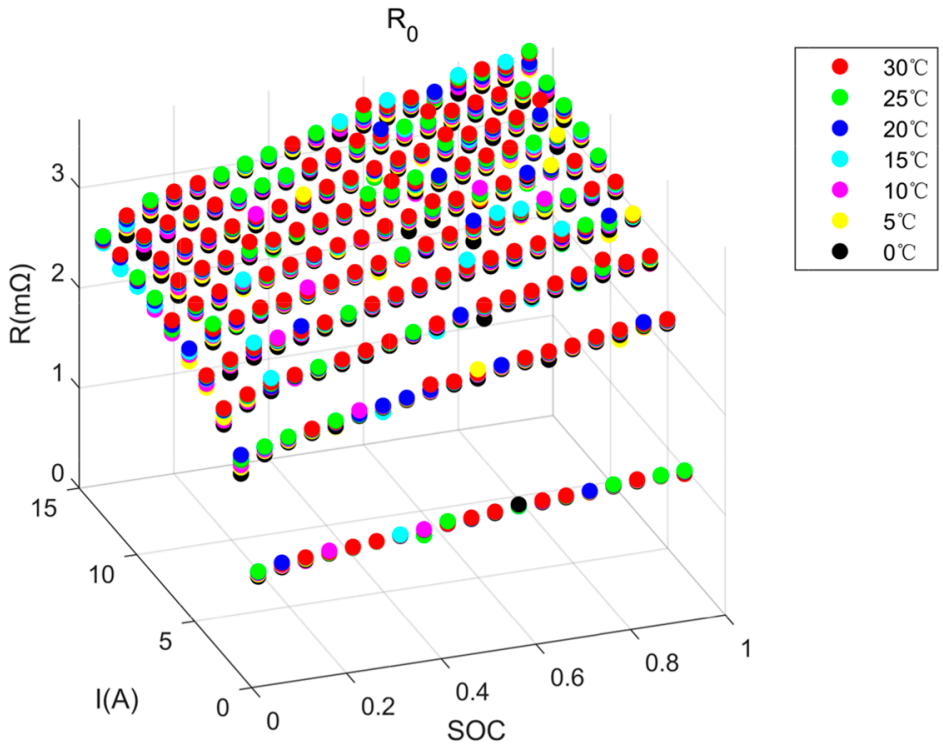


Figure 7. The variation in ohmic resistance corresponding to current and SOC at different temperatures.

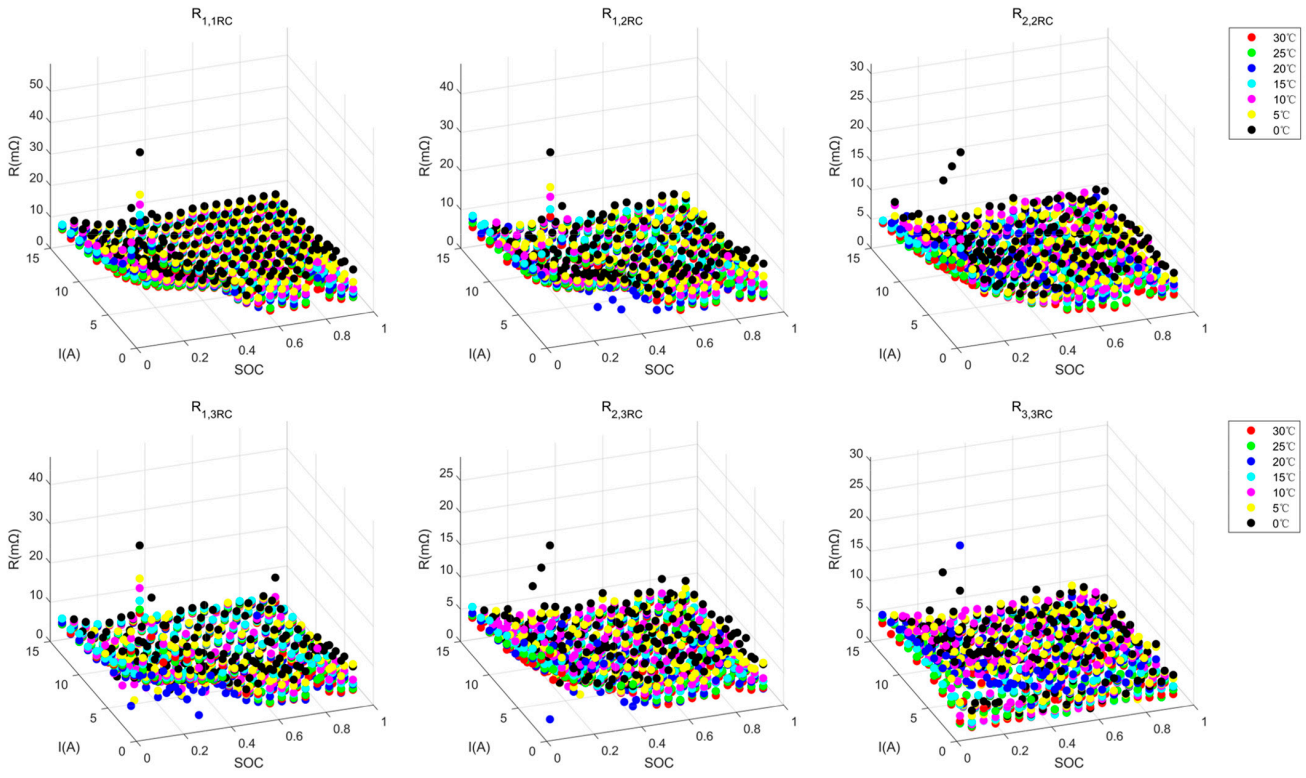


Figure 8. The variation in polarization resistance corresponding to current and SOC at different temperatures for models of various orders.

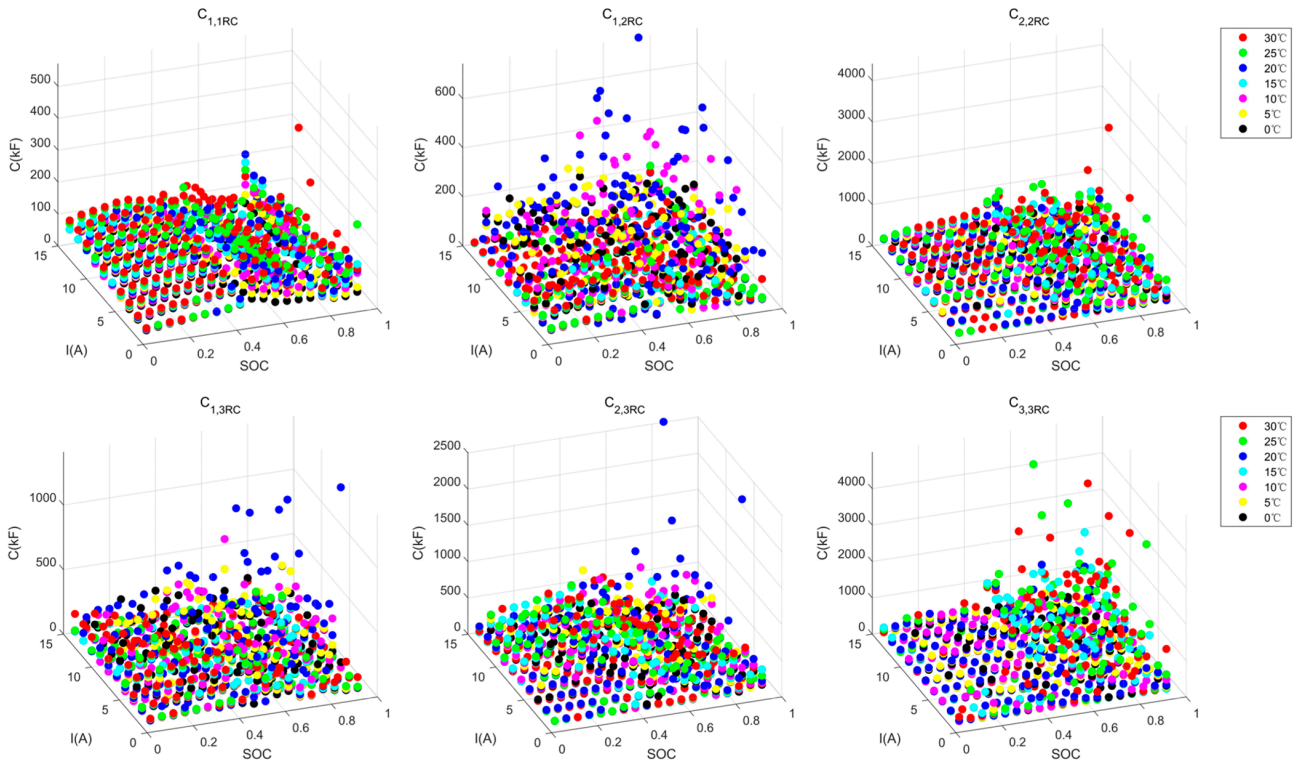


Figure 9. The variation in polarization capacitance corresponding to current and SOC at different temperatures for models of various orders.

5. Model Verification

Based on the terminal voltage formula of the model and the identified polarization resistance and capacitance, the simulated terminal voltage curves under different equivalent circuit models of the battery cell can be calculated. To ensure the accuracy and reliability of the models, the batteries discharged from a fully charged state to the discharge cutoff voltage with the discharge rate of 0.1 C (3 A), 0.2 C (6 A), 0.3 C (9 A), and 0.4 C (12 A), without applying temperature control. The terminal voltage, temperature, and current data were used for the verification in comparison with the simulated terminal voltage curves using the model.

To verify the superiority of the parameter identification method, we compared the root mean square error (RMSE%) of the terminal voltage calculated using the identified parameters with the RMSE% obtained using the unprocessed parameter acquisition method. The latter approach does not account for errors in sampling time during the identification process, nor does it consider the mutual constraints among the three models when calculating resistance and capacitance parameters. Through this comparison, a more practical model was selected for the soft-pack battery, thereby enhancing its application in stratospheric airship engineering.

Table 3 shows the terminal voltage curves obtained under different current conditions using two parameter identification methods. The root mean square errors (RMSE%) between the calculated terminal voltages from the first-order RC model, second-order RC model, and third-order RC model and the actual terminal voltage of the battery are presented in Table 4.

Table 3. Summary table of terminal voltage curves.

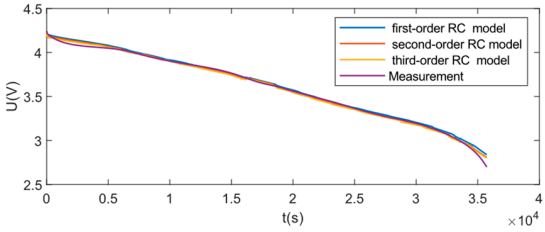
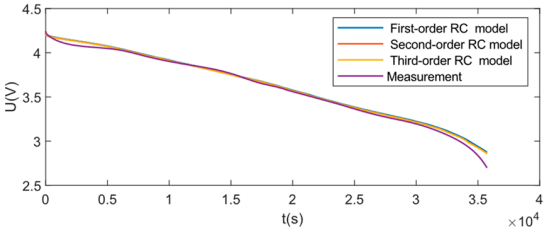
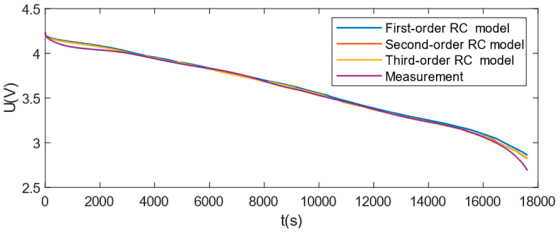
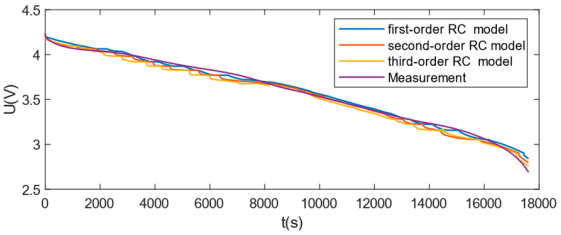
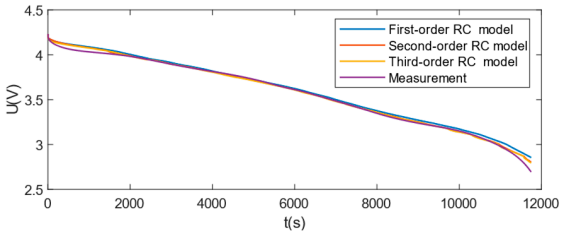
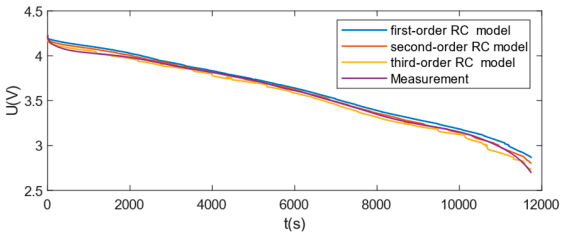
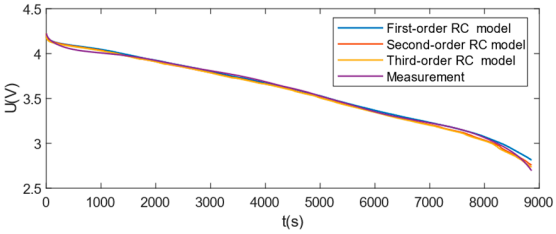
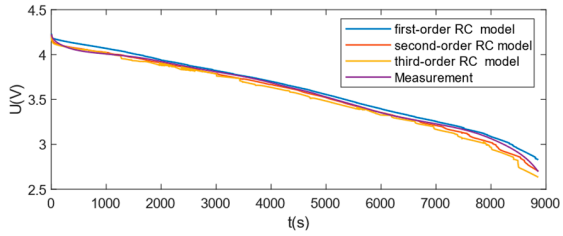
Discharge Rate	Terminal Voltage Curve Obtained from RC Parameters Calculated Considering Other Factors	Terminal Voltage Curve Obtained from RC Parameters Calculated Without Considering Other Factors
0.1 C		
0.2 C		
0.3 C		
0.4 C		

Table 3 shows that the terminal voltage curve obtained by incorporating additional factors into the resistance and capacitance parameters more accurately reflects the actual variations in the battery terminal voltage. In contrast, the curve derived without considering these factors exhibits noticeable fluctuations.

Table 4 shows that the root mean square error (RMSE%) of the terminal voltage calculated using parameters that include these factors is significantly lower than that calculated without them.

Therefore, the parameter identification method proposed in this paper significantly enhances model accuracy by systematically incorporating various influencing factors, allowing for a more precise description of the battery's dynamic characteristics.

Based on the accurately obtained resistance–capacitance (RC) parameter data, we conducted a comparative analysis of the root mean square error (RMSE) and runtime of various equivalent circuit models, with the results summarized in Table 5. All models were able to effectively demonstrate the dynamic characteristics of soft-pack batteries, though significant differences were observed in their specific performance.

Table 4. Summary of model errors with varying parameters.

Discharge Rate		First-Order RC Model		Second-Order RC Model		Third-Order RC Model	
		RMSE%	Improvement Value	RMSE%	Improvement Value	RMSE%	Improvement Value
0.1 C	Considering Other Factors	0.7064%	0.2524%	0.5460%	0.2828%	0.5220%	0.2813%
	Without Considering Other Factors	0.9588%		0.8288%		0.8033%	
0.2 C	Considering Other Factors	0.9385%	0.0209%	0.6513%	0.5038%	0.6174%	0.8179%
	Without Considering Other Factors	0.9594%		1.1551%		1.4353%	
0.3 C	Considering Other Factors	0.9634%	0.3679%	0.6053%	0.0509%	0.5400%	0.3210%
	Without Considering Other Factors	1.3313%		0.6562%		0.8610%	
0.4 C	Considering Other Factors	0.6072%	0.4606%	0.6063%	0.1277%	0.6983%	0.8414%
	Without Considering Other Factors	1.0678%		0.7340%		1.5397%	

Table 5. Summary of model errors and runtime based on accurate RC parameters.

Discharge Rate		0.1 C	0.2 C	0.3 C	0.4 C
RMSE%	First-order RC model	0.7064%	0.9385%	0.9634%	0.6072%
	Second-order RC model	0.5460%	0.6513%	0.6053%	0.6063%
	Third-order RC model	0.5220%	0.6174%	0.5400%	0.6983%
runtime	First-order RC model	0.0588 ms	0.0746 ms	0.0134 ms	0.0451 ms
	Second-order RC model	0.0596 ms	0.1060 ms	0.0138 ms	0.0793 ms
	Third-order RC model	0.0692 ms	0.1124 ms	0.0147 ms	0.0799 ms

In terms of modeling accuracy, the RMSE% of the first-order RC model was relatively high, indicating lower accuracy. The second-order RC model and the third-order RC model exhibited similar RMSE% values, both achieving high modeling accuracy. However, due to the more cumbersome parameter identification process of the third-order RC model and its insignificant error advantage, its efficiency and feasibility are limited in practical engineering applications.

From the perspective of runtime analysis, under the same discharge rate conditions, the first-order RC model had the shortest runtime due to its simple structure. The runtime of the second-order and third-order RC models was slightly longer than that of the first-order RC model, but the overall difference was minimal. All three models are capable of meeting the real-time requirements of engineering applications.

6. Conclusions

This study investigates the applicability and performance of aluminum–plastic film-encapsulated soft-pack lithium batteries for engineering applications in stratospheric airships. The effects of different temperatures and discharge rates on battery performance were evaluated using first-order, second-order, and third-order RC equivalent circuit models through constant-current intermittent discharge tests. By integrating the constraints among these models, comprehensive and accurate experimental data were collected.

The results indicate that the ohmic resistance of the soft-pack lithium battery remains stable, except for a significant decrease under low-current conditions. Temperature and the state of charge (SOC) minimally affect ohmic resistance. Polarization resistance remains stable but increases under low-current and low-SOC conditions. At low temperatures, polarization resistance is relatively higher, though the difference is not substantial. Polarization capacitance exhibits considerable fluctuation, but most values remain relatively stable.

To verify the advantages of the proposed parameter identification method, the root mean square error (RMSE%) of the terminal voltage calculated with the identified RC

parameters was compared to that obtained with unprocessed RC parameters. The results demonstrate that the RMSE% of the terminal voltage, after considering additional factors, is significantly smaller, highlighting the effectiveness of the proposed method.

There were no significant differences in the running time among the three models, all of which met engineering requirements. Although the first-order RC model has the shortest computation time, its error is relatively large. The second-order and third-order RC models exhibit similar errors, with RMSE% below 0.7%. Due to its higher computational load, the third-order RC model is less favored. Thus, the second-order RC equivalent circuit model was selected as the optimal choice in this study.

In summary, this study provides a theoretical foundation for the development and engineering of aluminum–plastic film-encapsulated soft-pack lithium batteries in high-specific-energy applications, enhancing their potential for use in stratospheric airships and other fields.

Author Contributions: Conceptualization, F.L. and Y.Z.; methodology, F.L.; software, F.L.; validation, X.W., G.X. and Z.L.; formal analysis, Y.Z. and Z.L.; investigation, F.L. and H.Z.; resources, Z.L. and X.W.; data curation, Y.Z.; writing—original draft preparation, F.L.; writing—review and editing, H.Z., Y.Z. and Z.L.; visualization, F.L.; supervision, Z.L., Y.Z. and G.X.; project administration, Z.L.; funding acquisition, Y.Z. All authors have read and agreed to the published version of the manuscript.

Funding: Postdoctoral Fellowship Program of CPSF (GZC20232762).

Data Availability Statement: The data presented in this study are available on request from the corresponding author due to privacy.

Conflicts of Interest: The authors declare no conflicts of interest.

References

1. Zhang, W.; Li, S.; Zhou, A.; Song, H.; Cui, Z.; Du, L. Recent Advances and Perspectives in Lithium−Sulfur Pouch Cells. *Molecules* **2021**, *26*, 6341. [CrossRef]
2. Jie, Y.; Tang, C.; Xu, Y.; Guo, Y.; Li, W.; Chen, Y.; Jia, H.; Zhang, J.; Yang, M.; Cao, R.; et al. Progress and Perspectives on the Development of Pouch-Type Lithium Metal Batteries. *Angew. Chem. Int. Ed. Engl.* **2024**, *63*, e202307802. [CrossRef]
3. Higashimata, A.; Adachi, K.; Hashizume, T.; Tange, S. Design of a headway distance control system for ACC. *JSAE Rev.* **2001**, *22*, 15–22. [CrossRef]
4. Zhao, W.; Zhao, Q.; Huang, J.; Hou, Z.; Du, Z. Application of near space solar powered UAV in modern war. *Air Space Def.* **2020**, *3*, 85–90. (In Chinese)
5. Stratospheric Airship Technology Authoring Team. *Stratospheric Airship Technology*; Science Press: Beijing, China, 2019; pp. 7–9. (In Chinese)
6. Song, K.; Li, Z.; Zhang, Y.; Wang, X.; Xu, G.; Zhang, X. Power Generation Calculation Model and Validation of Solar Array on Stratospheric Airships. *Energies* **2023**, *16*, 7106. [CrossRef]
7. Yuan, J.C.; Zhu, M.; Guo, X.; Lou, W. Trajectory tracking control for a stratospheric airship subject to constraints and unknown disturbances. *IEEE Access* **2020**, *8*, 31453–31470. [CrossRef]
8. Song, K.; Li, Z.; Zhang, Y.; Wang, X.; Xu, G.; Zhang, H. A rule-based online energy management strategy for long-endurance stratospheric airships. *Aerosp. Sci. Technol.* **2024**, *151*, 109266. [CrossRef]
9. Leng, M.; Liu, K.; Gao, Y.; Chen, H.; Yan, P.; Liu, X. Investigation of the electrical and thermal characteristics of soft-pack semi-solid-state lithium-ion batteries under high-rate discharge. *J. Energy Storage* **2024**, *97*, 112682. [CrossRef]
10. Zhang, X.; Zhang, W.; Lei, G. A Review of Li-ion Battery Equivalent Circuit Models. *Trans. Electr. Electron. Mater.* **2016**, *17*, 311–316. [CrossRef]
11. Wang, J.; Jia, Y.; Yang, N.; Lu, Y.; Shi, M.; Ren, X.; Lu, D. Precise equivalent circuit model for Li-ion battery by experimental improvement and parameter optimization. *J. Energy Storage* **2022**, *52*, 104980. [CrossRef]
12. Johnson, V.H. Battery performance models in ADVISOR. *J. Power Sources* **2002**, *110*, 321–329. [CrossRef]
13. Feng, Y.F.; Shen, J.N.; Ma, Z.F.; He, Y.J. Equivalent circuit modeling of sodium-ion batteries. *J. Energy Storage* **2021**, *43*, 103233. [CrossRef]
14. Zhang, K.; Xiong, R.; Li, Q.; Chen, C.; Tian, J.; Shen, W. A novel pseudo-open-circuit voltage modeling method for accurate state-of-charge estimation of $LiFePO_4$ batteries. *Appl. Energy* **2023**, *347*, 121406. [CrossRef]

15. Wu, J.; Xu, H.; Zhu, P. Lithium battery model online parameter identification method based on multi-innovation least squares. *Int. J. Model. Identif. Control* **2024**, *44*, 1–13. [CrossRef]
16. Liaw, B.Y.; Nagasubramanian, G.; Jungst, R.G.; Doughty, D.H. Modeling of lithium ion cells—A simple equivalent-circuit model approach. *Solid State Ion.* **2004**, *175*, 835–839.
17. Xia, B.; Sun, Z.; Zhang, R.; Lao, Z. A Cubature Particle Filter Algorithm to Estimate the State of the Charge of Lithium-Ion Batteries Based on a Second-Order Equivalent Circuit Model. *Energies* **2017**, *10*, 457. [CrossRef]
18. Wang, Q.; Wang, J.; Zhao, P.; Kang, J.; Yan, F.; Du, C. Correlation between the model accuracy and model-based SOC estimation. *Electrochim. Acta* **2017**, *228*, 146–159. [CrossRef]
19. Hu, X.; Li, S.; Peng, H. A comparative study of equivalent circuit models for Li-ion batteries. *J. Power Sources* **2012**, *198*, 359–367. [CrossRef]
20. Wang, W.; Zhang, L.; Zhang, J.; Yan, Y. Identification and verification of $LiFePO_4$ battery model parameters at high and low temperatures. *Chin. J. Power Sources* **2019**, *43*, 1464–1466+1491. (In Chinese)
21. Wang, W.; He, Y.; Sun, Y.; Yan, Y. Equivalent circuit model of lithium ion battery based on variable order RC network. *China Sci.* **2021**, *16*, 668–674. (In Chinese)
22. Wang, W.; Zhang, J.; Zhang, L.; Yan, Y. Equivalent circuit model for battery based on third-order RC network. *Battery Bimon.* **2019**, *49*, 212–216. (In Chinese)
23. Xia, F.; Yuan, B.; Peng, G.; Zhang, H. Modeling and Optimization of Variable-order RC Equivalent Circuit Model for Lithium Ion Batteries Based on Information Criterion. *Proc. CSEE* **2018**, *38*, 6441–6451+6506. (In Chinese)
24. Lin, P.; Liu, T.; Jin, P.; Wang, Z.; Wang, S.; Yuan, H.; Ma, Z.; Di, Y. Identification of lithium-ion battery equivalent circuit model parameters based on the multiinnovation identification algorithm. *Energy Storage Sci. Technol.* **2023**, *12*, 3155–3169. (In Chinese)
25. Amir, S.; Gulzar, M.; Tarar, M.O.; Naqvi, I.H.; Zaffar, N.A.; Pecht, M.G. Dynamic equivalent circuit model to estimate state-of-health of lithium-ion batteries. *IEEE Access* **2022**, *10*, 18279–18288. [CrossRef]
26. Pande, A.S.; Soni, B.P.; Bhadane, K.V. Electrical models for EV's batteries: An overview and mathematical design of RC network. *J. Inst. Eng. India Ser. B* **2023**, *104*, 533–547. [CrossRef]
27. Momma, T.; Matsunaga, M.; Mukoyama, D.; Osaka, T. Ac impedance analysis of lithium ion battery under temperature control. *J. Power Sources* **2012**, *216*, 304–307. [CrossRef]
28. Gomez, J.; Nelson, R.; Kalu, E.E.; Weatherspoon, M.H.; Zheng, J.P. Equivalent circuit model parameters of a high-power Li-ion battery: Thermal and state of charge effects. *J. Power Sources* **2011**, *196*, 4826–4831. [CrossRef]
29. Damodaran, V.; Paramadayalan, T.; Natarajan, D.; Kumar, C.R.; Kanna, P.R.; Taler, D.; Sobota, T.; Taler, J.; Szymkiewicz, M.; Ahamed, M.J. Development of a Fast Running Equivalent Circuit Model with Thermal Predictions for Battery Management Applications. *Batteries* **2024**, *10*, 215. [CrossRef]
30. Guo, J.; Guo, Q.; Liu, J.; Wang, H. The Polarization and Heat Generation Characteristics of Lithium-Ion Battery with Electric–Thermal Coupled Modeling. *Batteries* **2023**, *9*, 529. [CrossRef]
31. Yoganandan, H.; Srinivasan, K. Modeling and Validation of a Lithium-Ion Battery Pack. *J. Test. Eval.* **2023**, *51*, 2533–2552. [CrossRef]
32. Surya, S.; Samanta, A.; Williamson, S. Smart Core and Surface Temperature Estimation Techniques for Health-conscious Lithium-ion Battery Management Systems: A Model-to-Model Comparison. *Preprints* **2021**, *15*, 623. [CrossRef]
33. Wang, Q.; Gao, T.; Li, X. SOC Estimation of Lithium-Ion Battery Based on Equivalent Circuit Model with Variable Parameters. *Energies* **2022**, *15*, 5829. [CrossRef]
34. Bairwa, B.L.; Pareek, K.; Hampannavar, S.K. Investigation on lithium ion battery equivalent circuit models for dynamic load profiles. *Energy Storage* **2021**, *3*, e231. [CrossRef]
35. Barletta, G.; DiPrima, P.; Papurello, D. Thévenin's Battery Model Parameter Estimation Based on Simulink. *Energies* **2022**, *15*, 6207. [CrossRef]
36. Duru, K.K.; Venkatachalam, P.; Karra, C.; Madhavan, A.A.; Sambasivam, S.; Kalluri, S. Equivalent circuit model parameters estimation of lithium-ion batteries using cuckoo search algorithm. *J. Electrochem. Soc.* **2022**, *169*, 120503. [CrossRef]
37. Ji, Y.J.; Qiu, S.L.; Li, G. Simulation of second-order RC equivalent circuit model of lithium battery based on variable resistance and capacitance. *J. Cent. South Univ.* **2020**, *27*, 2606–2613. [CrossRef]
38. You, H.W.; Bae, J.I.; Cho, S.J.; Lee, J.M.; Kim, S.H. Analysis of equivalent circuit models in lithium-ion batteries. *AIP Adv.* **2018**, *8*, 125101. [CrossRef]
39. Pan, D.; Guo, H.; Tang, S.; Li, X.; Wang, Z.; Peng, W.; Wang, J.; Yan, G. Evaluating the accuracy of electro-thermal coupling model in lithium-ion battery via altering internal resistance acquisition methods. *J. Power Sources* **2020**, *463*, 228174. [CrossRef]

Disclaimer/Publisher's Note: The statements, opinions and data contained in all publications are solely those of the individual author(s) and contributor(s) and not of MDPI and/or the editor(s). MDPI and/or the editor(s) disclaim responsibility for any injury to people or property resulting from any ideas, methods, instructions or products referred to in the content.